# Low Resistance Tunnel Junctions for Efficient Electrically Pumped Nanolasers

Cheng-Yi Fang, Felipe Vallini, Abdelkrim El Amili, Joseph S. T. Smalley, *Member, IEEE*, and Yeshaiahu Fainman, *Fellow, IEEE* 

Abstract—Extremely compact nanoscale devices such as electrically pumped nanolasers are difficult to operate at room temperature due to the high electrical resistance inherent to small cavities. As a consequence, large voltages are necessary to reach the lasing threshold, which generates heat and reduces device efficiency. The poor heat sinking of small devices makes matters worse, dramatically reducing the laser efficiency. Instead of looking for solutions to dissipate heat from small structures more efficiently, designing nanolasers to produce less heat in the first place is an important goal. Here we propose and theoretically analyze the effect of adding an InGaAsP tunnel junction for efficient carrier injection in metallo-dielectric nanolasers. With our theoretical model we show that the device resistance is reduced by a factor of  $\sim$ 6.5. The applied voltage at the room temperature lasing threshold is reduced from 3.05 to 1.35 V, a reduction of 69% in heat generation, whereas the Q-factor and gain threshold of the cavity are not degraded.

Index Terms—Nanotechnology, semiconductor lasers, semiconductor device modeling, tunnel diodes, laser thermal factors.

#### I. INTRODUCTION

ANOSCALE semiconductor lasers have attracted growing interest because their small footprints may enable densely-packed chip-scale photonic circuits for various applications including optical interconnections, switching, sensing, displays and efficient lighting [1]. An essential requirement for many applications of nanolasers is electrical pumping at room temperature.

Among the various nanolaser designs, metallo-dielectric nanolasers are excellent candidates for optical sources in chipscale integrated circuits because of the mitigation of optical coupling between adjacent devices [2], smaller footprints than photonic crystal lasers [3], [4]; lower resistance current injection with respect to nanowire lasers [5], and lower cavity losses than metallic cavities [6], [7], plasmonic lasers [8] and spasers [9].

Manuscript received January 6, 2017; revised March 2, 2017; accepted March 2, 2017. This work was supported in part by the Office of Naval Research Multi Disciplinary Research Initiative; in part by the National Science Foundation (NNCI-SDNI, ERC CIAN); in part by the Defense Advanced Research Projects Agency; in part by the Army Research Office; and in part by Cymer Corporation.

C.-Y. Fang is with the Materials Science and Engineering Program, University of California at San Diego, La Jolla, CA 92093 USA (e-mail: c5fang@eng.ucsd.edu).

F. Vallini, A. E. Amili, J. S. T. Smalley, and Y. Fainman are with the Department of Electrical and Computer Engineering, University of California at San Diego, La Jolla, CA 92093 USA (e-mail: fvallini@eng.ucsd.edu; aelamili@eng.ucsd.edu; jsmalley@eng.ucsd.edu; fainman@ucsd.edu).

Color versions of one or more of the figures in this paper are available online at http://ieeexplore.ieee.org.

Digital Object Identifier 10.1109/JSTQE.2017.2679134

The main challenge in sub-wavelength lasers is to meet all the requirements for lasing emission while reducing the physical size of the device in all three dimensions. Indeed, shrinking the size of the resonator gives rise to a spatial spreading of the optical mode beyond its physical boundaries. This obviously induces a dramatic increase of the optical loss and thus increases the lasing threshold. To overcome this issue, one approach is to wrap the active medium with a combination of a dielectric shield and a metal layer [10]. By optimizing the thickness of the low index shield between the metal and semiconductor, the gain threshold of the laser can be substantially reduced. The benefit stems from the tendency of the low-index shield to push the electromagnetic mode towards the high-index inner core and away from the metal walls, reducing the mode metal overlap and hence, the Joule loss.

Because of their extreme compactness, nanolasers exhibit a large electrical resistance. Therefore, to reach lasing threshold, injecting current into the active region requires higher applied voltages. The generated Joule heat is detrimental to nanolasers and is one of the main limiting factors for room-temperature operation. Therefore, good thermal management and an efficient current injection scheme is necessary for nanolaser operation.

The best way to improve the current injection efficiency is to incorporate tunnel junctions into nanolasers as done in light emitting devices with much larger dimensions. For example, vertical cavity surface-emitting lasers (VCSELs) have suffered from poor current injection and spreading [11], [12], while lightemitting diodes (LEDs) have shown lower quantum efficiency and higher operation voltage than the theoretically predicted values [14]. These problems result from the small mobility of holes compared to electrons, which leads to p-contacts with high resistance. This issue is circumvented by replacing the p-type layers with more conductive layers. Therefore, tunnel junctions, formed by a heavily doped PN junction that allows electrons and holes to tunnel through the depletion region under negligible reversed bias, were introduced to replace the p-contact and improve the performance of VCSELs [11]-[13], LEDs [14]-[16] and, more recently, SOI-Integrated InP-based micro lasers [18], [19]. By incorporating tunnel junctions, both contacts are n-type materials which significantly alleviates current injection problems.

In this work, we demonstrate how the incorporation of a tunnel junction into our metallo-dielectric nanolaser design improves its electrical performance. We theoretically optimize the heterostructure, optical cavity and electrical properties. The

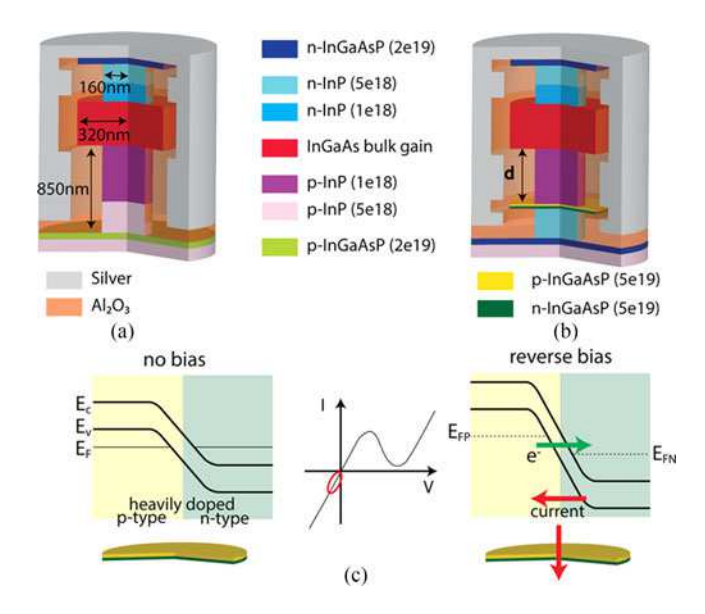


Fig. 1. Schematics of nanolasers (a) without and (b) with tunnel junction. (c) Reduced band diagram of a tunnel junction with no bias and reverse bias, and the respective IV curve.  $E_{\rm C}$  is the conduction band and  $E_{\rm V}$  is the valence band.  $E_{\rm F}$ ,  $E_{\rm FP}$  and  $E_{\rm FN}$  are the Fermi level, quasi-Fermi level for holes and quasi-Fermi level for electrons, respectively.

resistance of the device is reduced by a factor of  $\sim$ 6.5 compared to a design without a tunnel junction, which is a significant improvement in current injection efficiency. Finally we also show that the Joule heating is reduced by 69%.

The manuscript is organized as follows. In Section II, we provide the details of the epitaxial heterostructure design and illustrate how a tunnel junction can reduce the electrical resistance. In Section III, we use finite element method (FEM) simulations to show how the tunnel junction alters the quality factor, Q and threshold gain,  $g_{\rm th}$ , of the nanolaser. In Section IV, we extract the results from Section III and solve the laser rate equations to obtain the threshold carrier density. In Section V, we perform electrical simulations to estimate the efficiency improvement of the nanolaser with tunnel junctions. We further discuss the implications of using tunnel junctions on the nanolaser performance in Section VI.

### II. EPITAXIAL HETEROSTRUCTURE DESIGN

The schematic of the nanolaser under consideration is shown in Fig. 1. Fig. 1(a) corresponds to the design [20] of an electrically pumped metallo-dielectric nanolaser (labeled "device-O") without a tunnel junction. The gain medium consists of an intrinsic 320-nm-thick bulk InGaAs lattice matched to InP, which was predicted to be more suitable than InGaAsP multiple quantum wells nanolasers in terms of reducing threshold and single mode operation [21] Highly doped InGaAsP layers ( $2 \times 10^{19} \, \mathrm{cm}^{-3}$ ) on the bottom and top are the electrical contacts and doped InP layers serve as cladding layers through which the current is injected into the active layer. The radius of the gain medium and the InGaAsP contact layers is 320 nm. The 160-nm-undercut of the InP pedestals improves the mode quality factor, as discussed in [20]. The nanostructure is covered by an Al<sub>2</sub>O<sub>3</sub> dielectric layer to improve the thermal management followed by the sil-

ver layer added to improve the confinement [22]. The bottom p-InGaAsP and p-InP layers are poor conductors limiting the current injection efficiency. Since the mobility of holes is much lower than electrons, a high applied voltage is needed for current injection which tends to increase the Joule heating. The current injection resistance can be reduced by incorporating a tunnel junction into the nanolaser structure, as shown in Fig. 1(b). The tunnel junction consists of a heavily doped InGaAsP PN junction with 20-nm-thick p-InGaAsP and 12-nm-thick n-InGaAsP and it is placed below the p-InP (1  $\times$  10  $^{18}$  cm  $^{-3}$ ) cladding layer.

The working principle of a tunnel junction is illustrated by a reduced band diagram and the junction IV curve, both shown in Fig. 1(c). The doping concentration for both p- and n-type layers is  $5\times 10^{19}~\rm cm^{-3}$ . Such high doping concentration enables the Fermi level under equilibrium to be above the conduction band for n-type and below the valence band for p-type material without any bias. Since the depletion region is now extremely narrow, when a negligible reversed bias is applied, the Zener Effect enables a tunneling current through the junction. Therefore it is a conductive layer under negligible reverse bias. It is worth mentioning that in both Fig. 1(a) and (b) electrons are injected from the top and holes from the bottom which means when the device is under forward bias, the tunnel junction itself is under reverse bias.

It is worth to notice the IV curve of Fig. 1(c) corresponds to an applied voltage on the tunnel junction (not the entire device). Therefore, when the device is under reverse bias, even though the tunnel junction is under forward bias, the device can behaves as an insulator.

By incorporating the tunnel junction, we can replace the poorly conductive p-InGaAsP and p-InP (5  $\times$  10<sup>18</sup> cm<sup>-3</sup>) layers in Fig. 1(a) by n-InGaAsP and n-InP  $(5 \times 10^{18} \text{ cm}^{-3})$  layers in Fig. 1 (b), respectively. However, heavily doped tunnel junctions are lossy layers due to free carrier absorption. Indeed, the position of the junction must be properly chosen to optimize the nanostructure performance. The total thickness of InP layers between the InGaAs gain medium and the top of bottom p-InGaAsP contact is 850 nm. In Fig. 1(b), we define a variable "d" representing the distance between the bottom of the gain media to the top of the tunnel junction. Below the tunnel junction, p-type layers are replaced by n-type ones. In the following we investigate the influence of the tunnel junction position upon the cavity mode, i.e. when the tunnel junction is positioned at d = 125 nm (device-TJ-125) and d = 725 nm (device-TJ-725) from the optical mode.

A small resistance is expected with the device-TJ-125 but at the cost of a lower quality factor because of the mode overlap with the tunnel junction. In contrast, device-TJ-725has a lower overlap of the optical mode with the lossy tunnel junction layer increasing the quality factor of the optical mode. A more detailed analysis is addressed in the next section.

# III. OPTICAL CAVITY

To calculate the quality factor and confinement factor of the nanolasers, 3D simulations were carried out using the commercial FEM software (COMSOL). Usually the imaginary

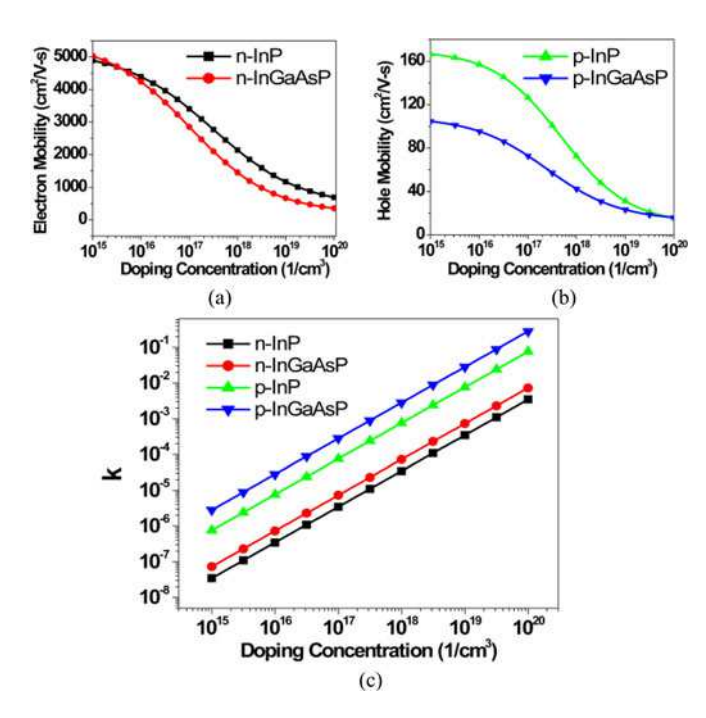


Fig. 2. Calculated (a) electron and (b) hole mobilities for n- and p- doped InP and InGaAsP, respectively, and the(c) imaginary part of their refractive index ( $\kappa$ ) for the different doping concentrations.

part of the refractive index  $(\kappa)$  is considered for metals but neglected for semiconductor and dielectrics because its values are much lower. However, the heavily doped tunnel junction is a highly absorbing layer due to its free carrier absorption. If  $\kappa$  is not considered, the simulated Q can be overestimated and consequently the calculated  $g_{\rm th}$  is underestimated.

Therefore, we employ the Drude (plasma) model to determine the loss,  $\alpha$ , and  $\kappa$ , which are related by the expressions: [23]

$$\Delta \alpha = \left(\frac{q^3 \lambda^2}{4\pi^2 c^3 \varepsilon_0 n}\right) \left[\frac{\Delta N_e}{m_{ee}^{*2} \mu_e} + \frac{\Delta N_h}{m_{eh}^{*2} \mu_h}\right] \tag{1}$$

$$\kappa = \frac{4\pi\alpha}{\lambda} \tag{2}$$

where q is the electronic charge, c is the speed of light,  $\varepsilon_0$  is the vacuum dielectric permittivity,n is the real part of the refractive index of the unperturbed material,  $m*_{ce/h}$  is the effective mass of electrons/holes,  $\mu_{e/h}$  is the electron/hole mobility and  $\Delta N_{/eh}$  is the electron/hole carrier density. The undoped InP and InGaAsP are considered transparent at the bulk gain media emission wavelength, so the free carrier absorption accounts for the loss just in the doped absorbing layers.

In equation (1), we have also considered a carrier dependent mobility model for electrons and holes. This model is described in detail in [24]. Fig. 2(a) and (b) show the electron and hole carrier density dependent mobility. It can be seen that the carrier mobility decreases when increasing doping concentration. Fig. 2(c) shows the calculated  $\kappa$  for InP and InGaAsP. The tunnel junction doping concentration of  $5 \times 10^{19} \, \mathrm{cm}^{-3}$  results in a  $\kappa$  of 0.014 and  $3.64 \times 10^{-4}$  for the p-InGaAsP and n-InGaAsP

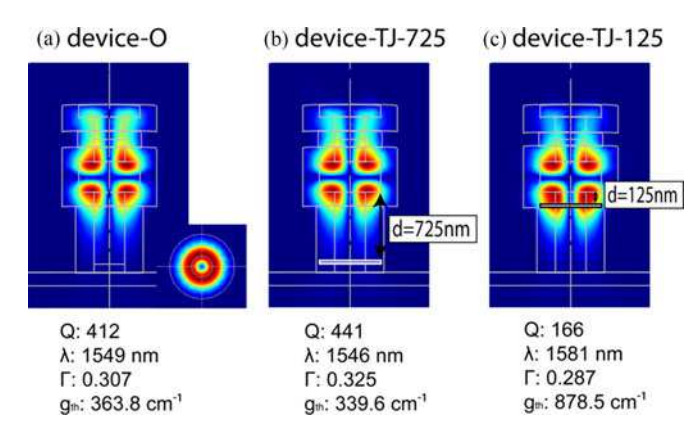


Fig. 3. Electric field of the lowest threshold mode,  $TE_{012}$ , for a nanolaser (a) without tunnel junction (device-O), (b) with a tunnel junction at d=725 nm (device-TJ-725) and (c) with a tunnel junction at d=125 nm (device-TJ-125).

layers, respectively. The mode overlap with the p-InGaAsP layer is then expected to decrease the Q-factor of the optical mode.

We performed 3D simulations by placing the tunnel junction beneath the gain media by d = 725 nm and d = 125 nm. Fig. 3 shows the electric field of the lowest threshold mode,  $TE_{012}$ , at a resonant wavelength within the material gain bandwidth and in the telecom C-band. The mode profile of a nanolaser without tunnel junction (device-O) is shown in Fig. 3(a). Fig. 3(b) and (c) are the nanolasers consisting of tunnel junctions with d = 725 nm and d = 125 nm,respectively (device-TJ-725 and device-TJ-125). The Q-factor, resonant wavelength  $(\lambda)$ , confinement factor ( $\Gamma$ ) and threshold gain ( $q_{\rm th}$ ) calculated as in [18] are also presented. If the tunnel junction is placed far enough from the gain media (device-TJ-725), shown in Fig. 3(b), the mode properties do not change significantly. In fact,  $\Gamma$ (0.325) and  $g_{\rm th}$   $(339.6~{\rm cm}^{-1})$  are superior than device-O. In Fig. 3(c) the optical mode is pulled down compared with Fig. 3(a) due to the high index InGaAsP tunnel junction.  $\Gamma$  drops from 0.307 to 0.287 and the mode overlap with the heavily doped tunnel junction also increases the loss resulting in lower Q and higher  $g_{\rm th}$ , which increases from 363.8 cm<sup>-1</sup> to 878.5 cm<sup>-1</sup>.

## IV. LASER RATE EQUATIONS

To obtain the threshold carrier density we then solve the laser rate equations, which are expressed as [25]:

$$\frac{dN}{dt} = R_{\text{pump}} - R_{\text{sp}} - R_{\text{sur}} - v_g g P \tag{3}$$

$$\frac{dP}{dt} = \Gamma v_g g P + \Gamma \beta R_{\rm sp} - \frac{\omega}{Q} P \tag{4}$$

where N is the carrier density, P is the photon density,  $R_{\text{pump}}$  is the pump rate by electronic injection,  $v_g$  is the group velocity,  $R_{\text{sp}}$  is the spontaneous emission rate and g is the material gain [26] where the detail of calculation can be found in [25].  $R_{\text{sur}}$  is the surface recombination rate which is critical to high surface to volume ratio nanoscale devices. The surface recombination velocity is assumed to be  $5 \times 10^4$  cm/s for InGaAs lattice matched to InP [21],  $\beta$  is the spontaneous emission coupling factor and  $\omega$ 

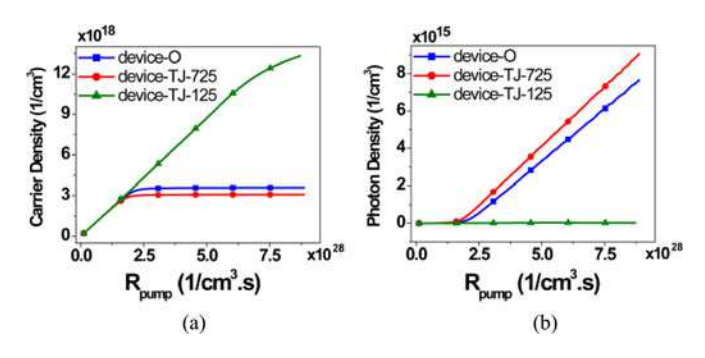


Fig. 4. (a) Carrier density and (b) output photon density evolution with the injection pumping rate for the three designs in consideration.

is the resonance frequency, which is extracted from COMSOL simulations in Fig. 3.

Fig. 4 shows the calculated carrier and photon density as a function of  $R_{\rm pump}$  in steady state. For nanolasers without a tunnel junction (device-O), the threshold carrier density is found to be  $3.5\times10^{18}~({\rm cm^{-3}})$ , while a tunnel junction 725 nm below the gain region (device-TJ-725) reduces the threshold carrier density to  $3.05\times10^{18}~({\rm cm^{-3}})$ . Fig. 4(b) shows that the slope efficiency for device-TJ-725 is higher than for device-O. However, a tunnel junction close to the gain region presents (device-TJ-125) a very high threshold due to the lower quality factor induced by free-carrier absorption. These results illustrate the importance of where to place the tunnel junction. With proper design, the threshold carrier density could be comparable or even better than without the tunnel junction.

## V. CURRENT INJECTION BEHAVIOR

To understand how tunnel junctions reduces the resistance, threshold voltage, and current, we used the commercial software SILVACO's ATLAS to predict the current injection through the heterojunction. SILVACO self-consistently solves the Poisson equation, the Schrodinger equation, and the carrier transport equations considering Fermi-Dirac statistics. We assumed perfect ohmic contacts for current injection, and the carrier density dependent mobility model (shown in Fig. 2(a) and (b)) was also incorporated into our simulations.

Fig. 5(a) shows the simulated IV curve. Device-TJ-725 outperforms device-O because of the low hole mobility, which impairs the current injection on device-O. Indeed, once a tunnel junction is introduced, the bottom p-InGaAsP contact is replaced by n-InGaAsP. Also, part of p-InP layer is replaced by n-InP [see Fig. 1(b)]. Because the electron mobility is two orders of magnitude larger than the hole mobility, to reach the same current, a much lower applied voltage is needed for device-TJ-725. The high resistance from p-type layers can be minimized; the device resistance is  $3372\Omega$  for device-O and  $519\Omega$  for Device-TJ-725. Therefore the tunnel junction reduces the injection current resistance by  $\sim$ 6.5 times.

From SILVACO, we can also extract the carrier density in the gain region with respect to applied voltages as shown in Fig. 5(b). To predict the threshold current, we related the results from laser rate equations to SILVACO simulations. In Fig. 4, we have

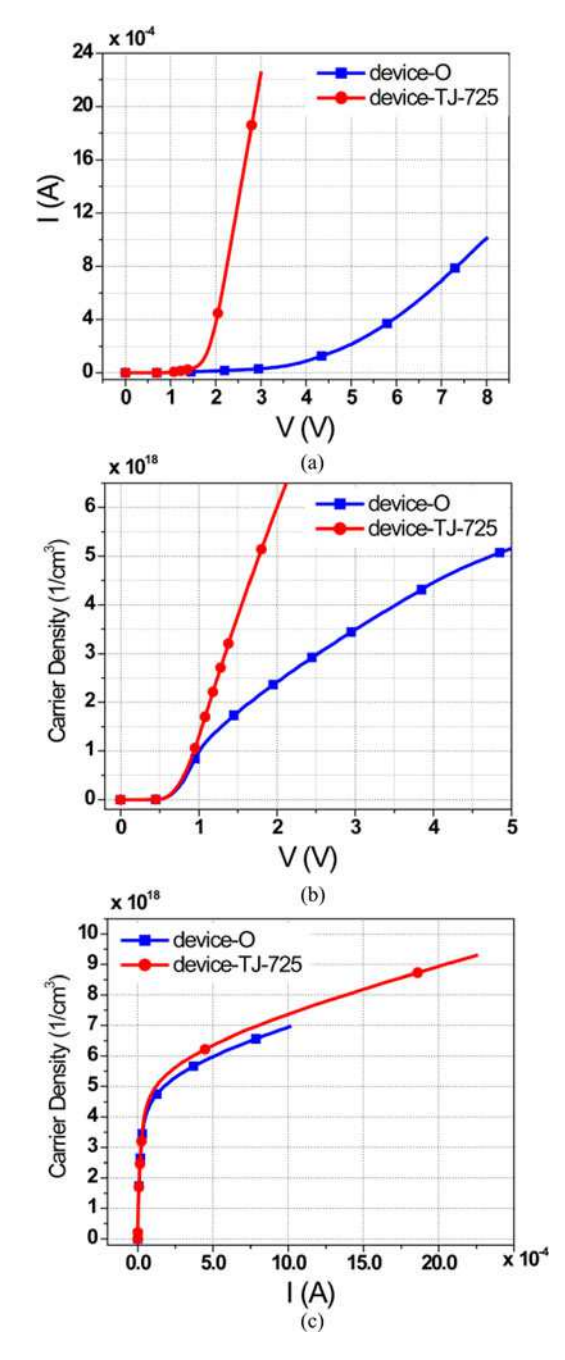


Fig. 5. (a) IV curve and (b) carrier density in the gain medium vs. applied voltage. (c) arrier density in the gain medium vs. injection current.

solved the rate equations at steady state to obtain the threshold carrier density for device-O  $(3.5 \times 10^{18} \, \mathrm{cm}^{-3})$  and device-TJ-725  $(3.05 \times 10^{18} \, \mathrm{cm}^{-3})$ . In Fig. 5(b), for device-O, 3.05 V is required to reach lasing threshold at room temperature. For device-TJ-725, which has n-InGaAsP on both ends as contact layers, only 1.35 V is needed to reach lasing threshold.

Fig. 5(c) shows the relation between the carrier density in the gain region and the current. The threshold current for device-TJ-725 is reduced by 31% compared to device-O. The two curves are almost identical below and above the threshold carrier density which means the reduced threshold current of device-TJ-725 results from a lower threshold carrier density.

TABLE I SIMULATED LASER CHARACTERISTICS FOR THE LOWEST THRESHOLD GAIN MODE OF DEVICES WITH DIFFERENT "d"

| d (nm)   | Q   | λ (nm) | Γ     | $g_{\mathrm{th}}\;(cm^{-1})$ | $N_{\rm th}  \times 10^{18}  (\text{cm}^{-3})$ | $V_{\rm th}$ (V) |
|----------|-----|--------|-------|------------------------------|------------------------------------------------|------------------|
| 125*     | 166 | 1581   | 0.287 | 878.5                        | X                                              | X                |
| 325      | 290 | 1551   | 0.306 | 519.6                        | 5.9                                            | 1.65             |
| 525      | 389 | 1546   | 0.319 | 385.0                        | 3.6                                            | 1.4              |
| 725*     | 441 | 1546   | 0.325 | 339.6                        | 3.05                                           | 1.35             |
| Device-O | 412 | 1549   | 0.307 | 363.8                        | 3.5                                            | 3.05             |

d = 125 nm is device-TJ-125; d = 725 nm is device-TJ-725;

#### VI. DISCUSSION

Inserting a heavily doped tunnel junction reduces the threshold voltage by 55% and current by 31%, leading to 69% reduction in power consumption and Joule heating. Room temperature nanolasers always suffer from self-heating due to the current injection. We had already proposed using  $Al_2O_3$  instead of  $SiO_2$  as the cladding layer for thermal management [22]. By incorporating a tunnel junction, thermal management can be further improved, which is necessary to realize stable room temperature nanolasers.

To optimize the structure, optimizing tunnel junction location is essential. Therefore understanding how "d" in Fig. 1(b) changes the cavity property and current injection is necessary in our design. We summarize the laser parameters in Table I. Optical characteristics calculated from COMSOL including  $Q, \lambda, \Gamma$  and  $g_{\rm th}$  are listed; threshold carrier density  $(N_{\rm th})$  from laser rate equations and threshold applied voltage  $(V_{\rm th})$  from SILVACO are also presented.

Table I shows the lossy tunnel junction position can be detrimental to the optical mode. The closer it is to the gain medium (smaller d), the smaller the Q is. On the other hand, placing a tunnel junction close to the gain region can reduce the amount of p-type layers and reduce the device resistance. There is indeed an inherent trade-off between the resistance and Q reduction as d is decreased. As an example, for device with d=325 nm,  $V_{\rm th}$  is 1.65 V which is 0.3 V higher than that with d=725 nm, showing that the resistance reduction does not compensate the Q reduction. Therefore, placing a tunnel junction far enough from the gain media is ideal to prevent optical mode overlap with the lossy layer for our metallo-dielectric nanolasers. To be more comprehensive, "d" can be used for optimization to find optimal performance in terms of Joule heating and gain threshold.

Moreover, because such high doping levels can be difficult to achieve experimentally, we have also analyzed the influence of tunnel junction with lower doping concentrations. We considered only the optimized device-TJ-725, but with tunnel junction doping concentrations of  $5\times 10^{18}~\rm cm^{-3}$ ,  $1\times 10^{19}~\rm cm^{-3}$  and  $2\times 10^{19}~\rm cm^{-3}$ . Since the tunnel junction is 725 nm below the gain region, the mode overlap with the tunnel junction was neglected. Therefore, we assume Q,  $\Gamma$  and  $g_{\rm th}$  do not change with the doping concentration of the tunnel junction in this case. The calculated threshold voltage are then 2.4 V, 1.75 V and 1.5 V, reducing the Joule heating by 44%, 60% and 62% respectively. These results show tunnel junctions are reliable even for lower doping concentrations.

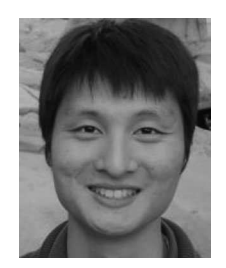
#### VII. CONCLUSION

In this article, we have analyzed the effect of incorporating a tunnel junction into our metallo-dielectric nanolasers. We proposed a new epitaxial structure and conducted optical and electrical modeling to theoretically demonstrate that electrical resistance of the device can be reduced without sacrificing the optical properties. By replacing the p-contact to form a PN tunnel junction 725 nm below the gain medium, the device resistance is reduced by a factor of  $\sim\!6.5$ . The applied threshold voltage is reduced from 3.05 V to 1.35 V and the threshold current by 31%, which results in a 69% reduction in Joule heating whereas the threshold gain for devices with and without tunnel junctions are comparable.

#### REFERENCES

- [1] Q. Gu et al., "Subwavelength semiconductor lasers for dense chip-scale integration," Adv. Opt. Photon., vol. 6, no. 1, pp. 1–56, Mar. 2014.
- [2] J. H. Lee et al., "Electrically pumped sub-wavelength metallo-dielectric pedestal pillar lasers," Opt. Express, vol. 19, no. 22, pp. 21524–21531, Oct. 2011.
- [3] O. Painter et al., "Two-dimensional photonic band-gap defect mode laser," Science, vol. 284, no. 5421, pp. 1819–1821, Jun. 1999.
- [4] H.-G. Park et al., "Electrically driven single-cell photonic crystal laser," Science, vol. 305, no. 5689, pp. 1444–1447, Sep. 2004.
- [5] M. H. Huang et al., "Room-temperature ultraviolet nanowire nanolasers," Science, vol. 292, no. 5523, pp. 1897–1899, Jun. 2001.
- [6] K. Ding and C. Z. Ning, "Metallic subwavelength-cavity semiconductor nanolasers," *Light Sci. Appl.*, vol. 1, no. 7, p. e20, Jul. 2012.
- [7] M.-K. Kim et al., "Engineering of metal-clad optical nanocavity to optimize coupling with integrated waveguides," Opt. Express, vol. 21, no. 22, pp. 25796–25804, Nov. 2013.
- [8] R. F. Oulton *et al.*, "Plasmon lasers at deep subwavelength scale," *Nature*, vol. 461, no. 7264, pp. 629–632, Oct. 2009.
- [9] M. A. Noginov et al., "Demonstration of a spaser-based nanolaser," Nature, vol. 460, no. 7259, pp. 1110–1112, Aug. 2009.
- [10] A. Mizrahi et al., "Low threshold gain metal coated laser nanoresonators," Opt. Lett., vol. 33, no. 11, pp. 1261–1263, Jun. 2008.
- [11] M. Ortsiefer et al., "Low-resistance InGa(Al)As tunnel junctions for long wavelength vertical-cavity surface-emitting lasers," Jpn. J. Appl. Phys., vol. 39, no. 4A, pp. 1727–1729, Apr. 2000.
- [12] S. Sekiguchi, T. Kimura, T. Miyamoto, F. Koyama, and K. Iga, "Long wavelength GaInAsP/InP laser with n-n contacts using AlAs/InP hole injecting tunnel junction," *Jpn. J. Appl. Phys.*, vol. 38, no. 4B, pp. L443– L445, Apr. 1999.
- [13] E. Kapon and A. Sirbu, "Long-wavelength VCSELs: Power-efficient answer," *Nature Photon.*, vol. 3, no. 1, pp. 27–29, Jan. 2009.
- [14] B. P. Yonkee *et al.*, "Demonstration of a III-nitride edge-emitting laser diode utilizing a GaN tunnel junction contact," *Opt. Express*, vol. 24, no. 7, pp. 7816–7822, Apr. 2016.
- [15] Y. Zhang et al., "Design and demonstration of ultra-wide bandgap AlGaN tunnel junctions," Appl. Phys. Lett., vol. 109, no. 12, Sep. 2016, Art. no. 121102.
- [16] M. X. Feng et al., "High efficient GaN-based laser diodes with tunnel junction," Appl. Phys. Lett., vol. 103, no. 4, Jul. 2013, Art. no. 043508.
- [17] M. J. Grundmann and U. K. Mishra, "Multi-color light emitting diode using polarization-induced tunnel junctions," *Phys. Status Solidi C*, vol. 4, no. 7, pp. 2830–2833, Jun. 2007.
- [18] J. V. Campenhout et al., "A compact SOI-integrated multiwavelength laser source based on cascaded InP microdisks," *IEEE Photon. Technol. Lett.*, vol. 20, no. 16, pp. 1345–1347, Aug. 2008.
- [19] J. V. Campenhout et al., "Electrically pumped InP-based microdisk lasers integrated with a nanophotonic silicon-on-insulator waveguide circuit," Opt. Express, vol. 15, no. 11, pp. 6744–6749, 2007.
- [20] J. Shane, Q. Gu, A. Potterton, and Y. Fainman, "Effect of undercut etch on performance and fabrication robustness of metal-clad semiconductor nanolasers," *IEEE J. Quantum Electron.*, vol. 51, no. 1, Jan. 2015, Art. no. 2000109.

- [21] F. Vallini, Q. Gu, M. Kats, Y. Fainman, and N. C. Frateschi, "Carrier saturation in multiple quantum well metallo-dielectric semiconductor nanolaser: Is bulk material a better choice for gain media?" *Opt. Express*, vol. 21, no. 22, pp. 25985–25998, Nov. 2013.
- [22] Q. Gu et al., "Amorphous Al2O3 shield for thermal management in electrically pumped metallo-dielectric nanolasers," *IEEE J. Quantum Electron.*, vol. 50, no. 7, pp. 499–509, Jul. 2014.
- [23] P. K. Basu, Theory of Optical Processes in Semiconductors: Bulk and Microstructures, 1st ed. Oxford, U.K.: Oxford Univ. Press, 2007.
- [24] M. Sotoodeh, A. H. Khalid, and A. A. Rezazadeh, "Empirical low-field mobility model for III–V compounds applicable in device simulation codes," *J. Appl. Phys.*, vol. 87, no. 6, Mar. 2000, Art. no. 2890.
- [25] S.-L. Chuang, Physics of Photonic Devices, 2nd ed. Hoboken, NJ, USA: Wiley, 2009.
- [26] J. S. T. Smalley, Q. Gu, and Y. Fainman, "Temperature dependence of the spontaneous emission factor in subwavelength semiconductor lasers," *IEEE J. Quantum Electron.*, vol. 50, no. 3, pp. 175–185, Mar. 2014.



**Cheng-Yi Fang** received the B.S. and M.S. degrees from National Taiwan University, Taipei, Taiwan.

He is currently working toward the Ph.D. degree in the Ultrafast and Nanoscale Optics Group, University of California, San Diego, San Diego, CA, USA. His research interests include photonics, semiconductor lasers and plasmonics.



**Felipe Vallini** received the B.S., M.S., and Ph.D. degrees in physics from the State University of Campinas, Campinas, Brazil, in 2007, 2009, and 2013, respectively.

He has completed research internship as a Visiting Scholar with the University of California San Diego (UCSD), La Jolla, CA, USA. He is currently a Postdoctoral Researcher at UCSD. His researcher interests include design, fabrication, and characterization of semiconductor nanolasers and plasmonic nanolasers, solid-state physics, and nanophotonics.



Abdelkrim El Amili received the B.Sc. degree in physics and engineering and the M.Sc. degree in fundamental physics from the University of Bordeaux 1, Bordeaux, France, in 2004 and 2006, respectively, and the Ph.D. degree in physics from the University of Paris-Sud XI, Orsay, France, in 2010. His thesis work was on the realization of an experimental setup for atoms detection in atom on a chip, and on the theoretical investigation of detection performances of coupled micro-cavities.

He is currently a Physicist specialized in optics and laser physics. From 2010 to 2011, he worked as a Postdoctoral Researcher in laser physics at the Laboratoire Aimé Cotton, Paris, and from 2011 to 2014, he worked as a Nonpermanent Researcher in the Institut de Physique de Rennes 1, CNRS-University of Rennes 1. His research interests include the experimental and theoretical study of the dynamics of solid-state lasers. Particularly, he was focused on the development of optical methods enabling a strong suppression of inherent resonant intensity noises in single-/dual-frequency solid-state lasers. He joined Professor Yeshaiahu Fainman's research group in January 2015, where he is currently working as an Assistant Project Scientist. His research interests include both III–V and Silicon technologies.



**Joseph S. T. Smalley** (M'10) received the B.S. degree in engineering science from Pennsylvania State University, State College, PA, USA, in 2011, and the M.S. and Ph.D. degrees in electrical engineering (nanoscale devices and systems) from the University of California San Diego (UCSD), La Jolla, CA, USA, in 2013 and 2016, respectively.

In 2015, he was a Visiting Researcher at the Center for Integrated Nanotechnologies, Sandia National Laboratory, Albuquerque, NM, USA. He is currently a Postdoctoral Researcher at UCSD. His research in-

terests include the fundamental theory, design, fabrication, and characterization of nanophotonic devices, such as gain-enhanced metamaterials and nanoscale light sources, as well as the conceptualization and design of photonic systems for Smart City applications.



Yeshaiahu Fainman (F'03) received the M.Sc. and Ph.D. degrees from Technion—Israel Institute of Technology, Haifa, Israel, in 1979 and 1983, respectively.

He is currently a Cymer Professor of advanced optical technologies and a Distinguished Professor in electrical and computer engineering at the University of California San Diego (UCSD), La Jolla, CA, USA. He is directing research of the Ultrafast and Nanoscale Optics group at UCSD and made significant contributions to near-field optical phenomena.

nanophotonics and plasmonics, and nonconventional imaging. The research applications target information technologies and biomedical sensing. He contributed more than 250 manuscripts in peer-review journals and more than 450 conference presentations and conference proceedings.

Dr. Fainman is a Fellow of the Optical Society of America and the International Society for Optics and Photonics, and received the Miriam and Aharon Gutvirt Prize, the Lady Davis Fellowship, the Brown Award, the Gabor Award, and the Emmett N. Leith Medal.